Osteonecrosis of the Upper Extremity: MRI-Based Zonal Patterns and Differential Diagnosis

Rainer Schmitt, MD, PhD[1,2] K.H. Kalb, MD[3] G. Christopoulos, MD[1] J.P. Grunz, MD[1,2]

[1] Department of Radiology, Rhön-Klinikum AG, Bad Neustadt, Germany
[2] Department of Radiology, University Hospital Würzburg, Würzburg, Germany
[3] Department of Hand Surgery, Rhön-Klinikum AG, Bad Neustadt, Germany

Address for correspondence Rainer Schmitt, MD, PhD, Rankestraße 51 b, D-85051 Ingolstadt, Germany (e-mail: radiodiagnostics@outlook.com).

Semin Musculoskelet Radiol 2019;23:523–533.

Abstract

Regarding the upper extremity, osteonecrosis can relate to the humeral head and to any carpal bone, most commonly the lunate (Kienböck's disease), scaphoid (Preiser's disease and nonunion), and capitate bone (osteonecrosis of the capitate head). In children and adolescents, osteochondrosis is an important differential diagnosis at the epiphyses. Appropriate imaging of osteonecrosis depends on knowledge about blood supply, biomechanical load, and bone repair mechanisms. Contrast-enhanced MRI (ceMRI) enables the differentiation of up to three mostly band-shaped zones: necrotic tissue (proximal), hypervascular repair tissue (intermediate), and viable bone (distal). To distinguish between necrotic and repair zones, intravenous gadolinium is recommended in MRI. Osteosclerosis and insufficiency fractures in early and intermediate stages as well as osteoarthritis in advanced stages are best depicted using high-resolution CT (HRCT). The combination of HRCT and ceMRI allows for exact classification of osteonecrosis regarding morphology and viability.

Keywords
- carpus
- gadolinium
- MRI
- osteochondrosis
- osteonecrosis

Osteonecroses of the Carpal Bones

Pathoanatomy

Osteonecrosis is primarily based on ischemia with loss of osteocytes, followed by secondary changes in the remaining bone, particularly the mineralized osteoid. Osteonecrosis occurs, in contrast to bone infarction, at the epiphyses of a bone, which can be explained by their special vascularization. Occlusion of arterial vessels and consecutive loss of blood supply are the main causes of osteonecrosis. The carpalia are particularly at risk of osteonecrosis due to their distinctive retrograde vascularization pattern.[1–3] Therefore, the proximal poles' blood supply is comparatively low, thus rendering the proximal bone segments vulnerable to carpal osteonecrosis.

Several causes of reduced perfusion are discussed. Chronic repetitive trauma, for example, is assumed to predispose a person to intraosseous artery occlusion.[4] Blood supply may be interrupted by fractures,[5] for example, proximal scaphoid fracture or nonunion leading to secondary osteonecrosis. Venous stasis may also contribute to the development of osteonecrosis because intraosseous hypertension was found in several cases of Kienböck's disease.[6] In addition to vascular causes, biomechanical circumstances play a role in the development of osteonecrosis.[7–9]

Besides the presence of avital bone tissue, extensive osseous remodeling takes place in carpal osteonecrosis.[5,10–12] Under the influence of different initiating and modulating factors, neovascularization is stimulated, and blood vessels begin to form from viable tissue to the ischemic areas.[13,14] The emergence of reparative fibrovascular tissue leads to the formation of an intermediate zone between necrosis and viable bone (►**Fig. 1b**). In juvenile osteonecrosis, the reparative tissue may be completely transformed into lamellar bone over time,

Rainer Schmitt's ORCID is https://orcid.org/0000-0001-9571-6332.

Issue Theme Imaging Around the Ends of Bones; Guest Editor, Christian Glaser, MD

DOI https://doi.org/10.1055/s-0039-1695719.
ISSN 1089-7860.

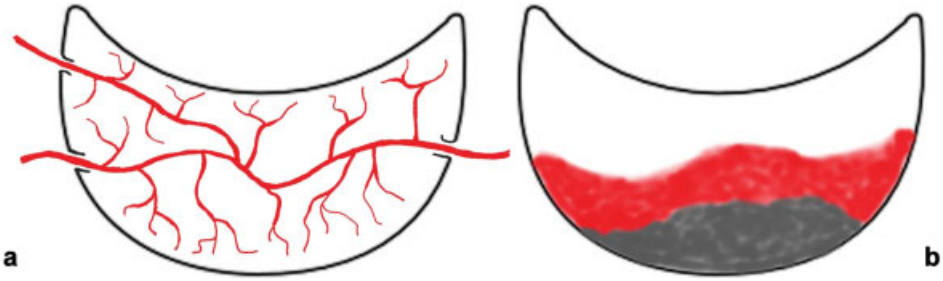

Fig. 1 Vascular supply of the lunate and zones of lunate necrosis. (**a**) The nutrient vessels enter the lunate via the anterior and posterior horns and form a retrograde intraosseous vascular network. Thus the proximal lunate section becomes the vascular terminal zone. (**b**) This results in a zonal structure in lunate necrosis: the necrosis zone is located proximal (shown in gray), the hypervascularized repair zone in the middle (shown in red), and the zone of remaining vitality distal (shown in white).

sometimes resulting in minor deformity.[15] In the adult form of carpal osteonecrosis, the reparative process is usually incomplete. Thus avital bone persists alongside viable tissue.

Reparative hyperemia typically facilitates regional osteopenia through hyperactivity of bone metabolism that in turn favors the occurrence of pathologic fractures and articular damage. The resulting osteoarthrosis can be progredient over a long time, occasionally leading to carpal collapse with significant loss of carpal height.[16,17]

Necrotic carpal bones regularly display a three-layered composition with three different histologic zones (►**Fig. 1b**)[13,18–20]:

- *Proximal zone of necrosis:* The largest extension of osteonecrosis is normally located in the proximal segments of the lunate, scaphoid, and capitate bone due to limited blood supply and high axial load. In case of failed repair, osteosclerosis is commonly found in these areas because of insufficient osteoclast functioning. By contrast, the overlaying articular cartilage stays mostly intact.
- *Intermediate zone of repair:* The layer between proximal necrosis and distal viability consists of intensely perfused fibrovascular tissue, regions of osteopenia, and sometimes (pathologic) fractures. This zone resembles a nonunion filled with connective tissue.
- *Distal zone of viable bone:* The distal poles of the lunate, scaphoid, and capitate bone are less vulnerable to ischemia because of their favorable perfusion conditions; thus they are usually composed of viable bone marrow and osseous tissue.

Osteonecrosis of the Lunate Bone (Kienböck's Disease)

Vascularization of the lunate depends on nutrient vessels from the radial artery for the posterior horn and nutrient vessels from the ulnar and anterior interosseous artery for the anterior horn. These arteries traverse through the lunate in a retrograde direction (►**Fig. 1a**). Assumed causes of osteonecrosis include repetitive[4] or onetime[5,6] trauma, different metabolic and endocrinologic conditions, and ulna minus variants,[8,9] where the radial part of the proximal lunate bone is exposed to increased axial load. The juvenile form of Kienböck's disease shows better prognosis for revascularization and healing than the adult form.[15]

Treatment of Kienböck's disease depends on several factors: (1) stage of necrosis, (2) ulna variance (assessed with plain radiography in neutral position of the wrist), (3) degree of osteoarthritis in the radiocarpal joint, and (4) patient age.

Conventional radiography displays several distinctive findings:[21]

- According to Hultén,[7] Kienböck's disease is found frequently in conjunction with ulna minus variants that result in increased axial load on the radial part of the lunate.
- Osteoclasts are more sensitive to ischemia than osteoblasts, which leads to inhibition of bone resorption and regional osteosclerosis.[19]
- Deformation of necrotic bone occurs due to insufficiency fractures in the repair zone. Impaction commonly affects the proximal-radial part of the lunate.[19]
- After impaction, loss of carpal height can be quantified using the indices of Youm et al (carpal height divided by the height of the metacarpal bone III; reference value 0.54 ± 0.03) and Nattrass[22] (carpal height divided by the height of the capitate bone; reference value 1.57 ± 0.05).[23] Development of osteoarthritis usually affects the radiocarpal and later midcarpal joints.

Computed tomography (CT) (slice thickness < 1 mm) is superior to radiography in visualizing the internal structure and articular surfaces of carpal bones[18,19,24]:

- Because of its high resolution, CT depicts osteosclerosis and pseudocysts (stage II) as well as fracture lines at the proximal circumference of the lunate (stage IIIa) earlier and more reliably than plain radiography.[17,24]
- Sagittal multiplanar reformation (MPR) is most suitable for displaying coronal fractures (stage IIIc) of the lunate bone (►**Fig. 3a**, **b**, ►**Fig. 4a**, **b**).
- Osteophytes, subchondral sclerosis, and articular joint asymmetries are typical features of stage IV of Kienböck's disease (►**Fig. 4a**, **b**).[19]

Magnetic resonance imaging (MRI) mainly displays the fat cells that contribute to the high signal of the bone marrow. Every change to the signal hints at remodeling of the bone marrow.[25] Medullary signal changes may point to disorders of bone metabolism.[10] Fat cells survive the bone marrow edema usually caused by ischemia only for a limited period of 2 to 5 days. Coincident with the onset of osteonecrosis, repair

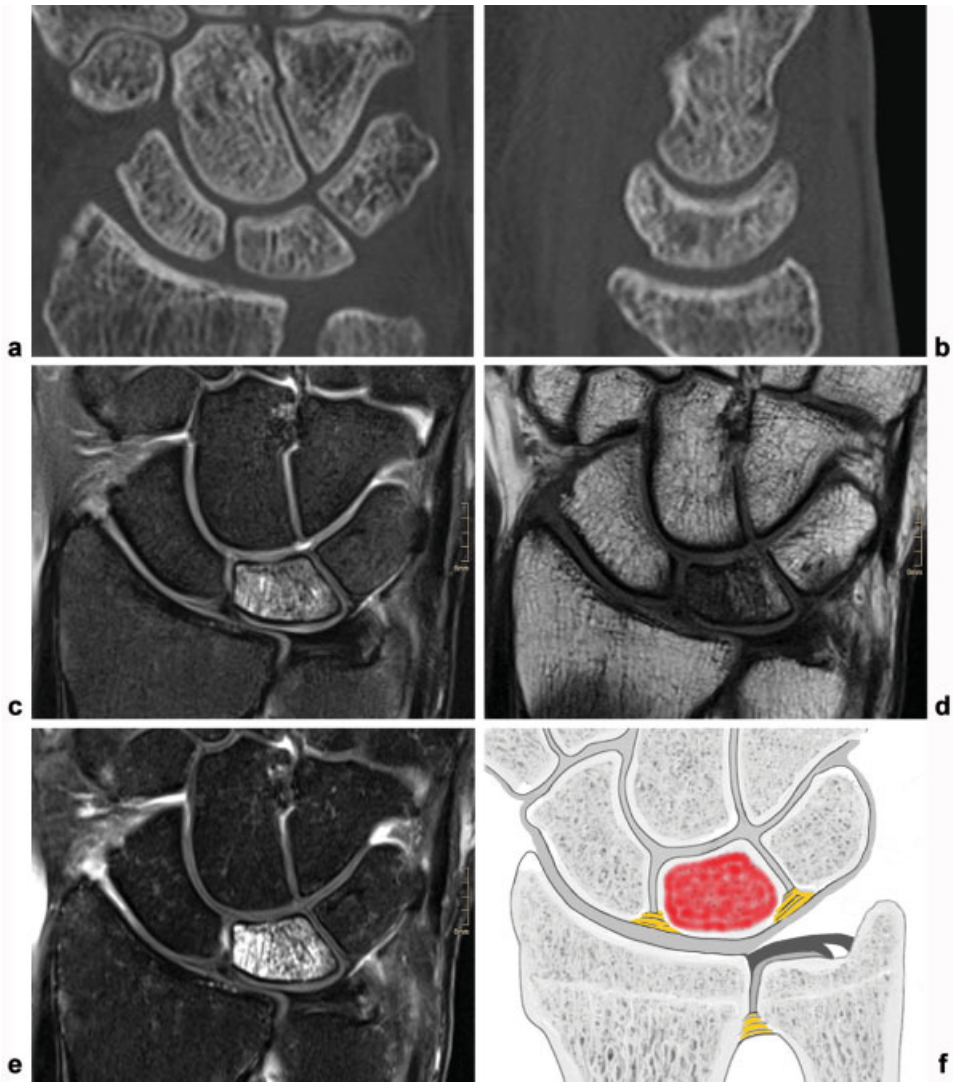

Fig. 2 Computed tomography CT) and magnetic resonance imaging findings in perfusion pattern A of lunate necrosis. (**a**, **b**) In high-resolution CT (coronal and sagittal multiplanar reformation), the lunate is inconspicuous in terms of shape as well as cortical and trabecular structure. (**c**, **d**) Territorial bone marrow edema in the lunate with radial focus of intensity, hyperintense in coronal intermediate proton-density fast spin-echo (FSE) fat saturated (c), and hypointense in coronal T1 FSE plain (d). (**e**, **f**) Strong hyperenhancement in the lunate (e) after gadolinium application (contrast-enhanced T1 FSE fat saturated). The territorial hyperenhancement is shown in red in the schematic picture (f).

processes are initiated, and by activation of osteoblasts and osteoclasts, bone remodeling is induced.[26]

- In plain MRI, the different phases of osteonecrosis can be distinguished by means of the specific relaxivity of participating tissues.[10,11,14,26,27] Ischemic bone marrow edema leads to loss of T1 and increase of T2 signal (►**Fig. 2c**, **d**). The loss of fat cells results in signal loss in T1- and T2-weighted sequences (►**Fig. 3c**, **d**, ►**Fig. 4c**, **d**). Further contributing to the overall signal loss are the emergence of fibrovascular tissue, increasing osteosclerosis of trabecular bone and fragment impaction.
- In contrast-enhanced MRI, perfusion of bone marrow can be assessed with T1 relaxation times.[18,20,28,29] Viable bone marrow shows no enhancement, whereas fibrovascular repair tissue presents significant hyperenhancement due to hyperemia in contrast-enhanced magnetic resonance imaging (ceMRI) (►**Fig. 2f**).[18,20] The mesenchymal repair attempt can be detected on the basis of gadolinium enhancement at the distal margin of osteonecrosis. Therefore, differentiation of the following zonal anatomy is usually feasible: (1) *Necrotic bone marrow* with hypointense signal in plain MRI and no gadolinium enhancement in ceMRI. (2) *Fibrovascular repair tissue* with hypointense signal in plain MRI and intense gadolinium enhancement in ceMRI. (3) *Viable bone marrow* with regular signal intensity in plain MRI and no gadolinium enhancement in ceMRI.

Lichtman's staging system: By the implementation of CT and MRI, the traditional classification of Decoulx et al[21] is modified in several ways[23,30,31]:

- Stage I is characterized by the presence of bone marrow edema besides viable osseous tissue. This "occult" stage can only be detected with MRI. Shape and internal structure of the lunate are unremarkable in radiography and CT imaging.

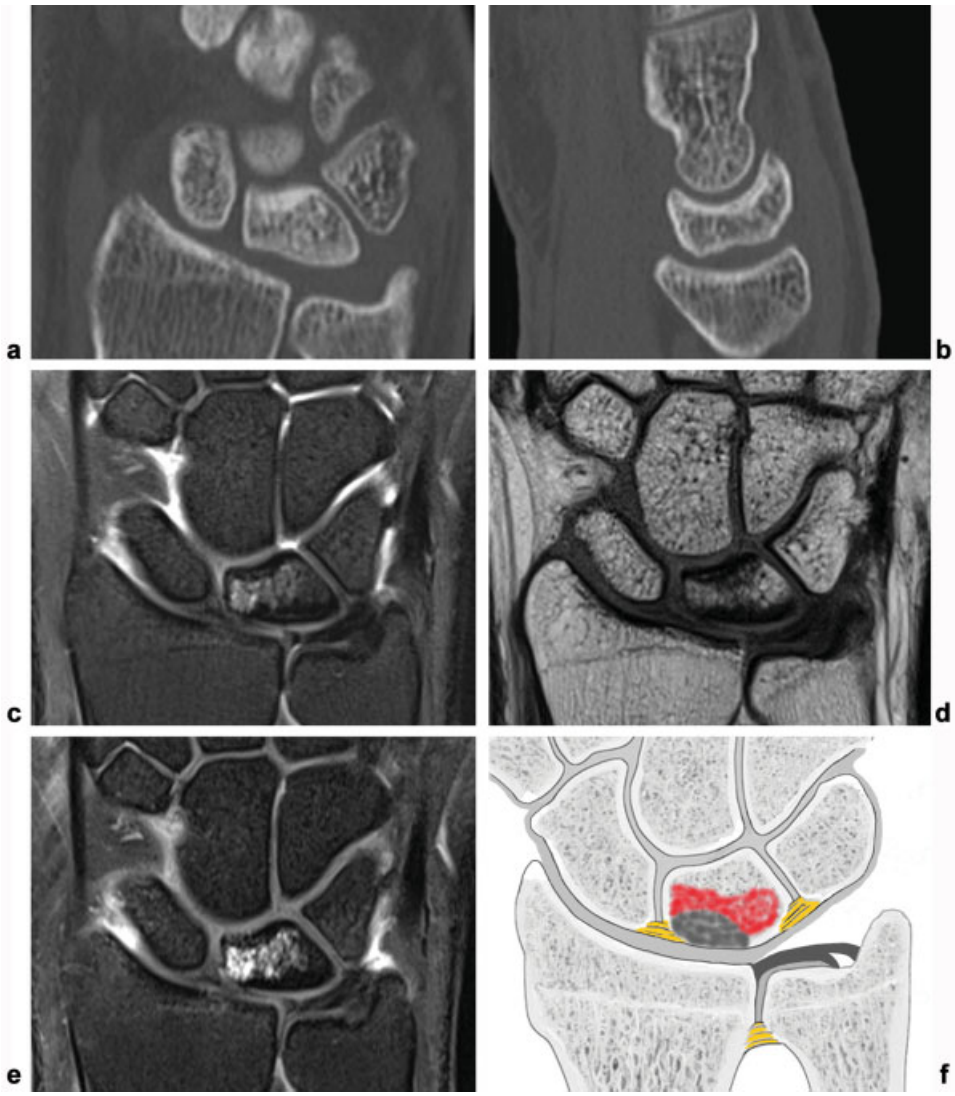

Fig. 3 Computed tomography (CT) and magnetic resonance imaging findings in perfusion pattern B of lunate necrosis. (**a**, **b**) CT imaging (coronal and sagittal multiplanar reformation) shows an impaction of the lunate with irregular shape of its proximal circumference. The loss of height is located in the radial half of the lunate. (**c**, **d**) Fat-saturated proton-density fast spin-echo (FSE) (c) and plain T1 FSE (d) show a narrow, hypointense zone at the proximal circumference with adjacent zonal bone marrow edema in large parts of the lunate. (**e**, **f**) Fat-saturated T1 FSE scan after gadolinium application (e) depicts missing enhancement in the proximal lunate; strong hyperenhancement is present in the edema zone as an expression of increased perfusion. The schematic drawing (f) shows the underlying pathology with proximal necrosis, intermediate reparation, and distal viability zone.

- Stage II is marked by regional osteosclerosis alongside cystic lesions, expressing an imbalance between osteoclast and osteoblast activity. The shape of the lunate remains normal.
- Stage III describes insufficiency fractures of the necrotic lunate bone. Although no significant impaction is present at first (stage IIIa), later stages are characterized by considerable loss of carpal height and flexion position of the scaphoid (stage IIIb). The index of Youm et al (reference value 0.54 ± 0.05) and assessment of the scapholunate angle (reference value < 60 degrees) facilitate the differentiation between stages IIIa and IIIb. The presence of a coronal fracture is referred to as stage IIIc.
- Stage IV displays radiography criteria of osteoarthritis due to long-time compromised biomechanical stability of the carpus.

MRI viability pattern: By means of ceMRI, relaxivity of bone marrow is evaluated before[10,11,14,26,27] and after[18,19] application of a gadolinium-based contrast agent. Particularly relevant for prognosis is the remaining perfusion condition in the proximal zones of the lunate. In Kienböck's disease, three different MRI patterns can be discerned:

- MRI pattern A (►**Fig. 2**): The distinctive feature of this pattern is the presence of bone marrow edema while osteocyte function, blood supply, and bone structure remain intact. Because of maintained perfusion or neovascularization in the proximal part of the lunate, homogeneous gadolinium hyperenhancement is found after application of contrast agent.
- MRI pattern B (►**Fig. 3**): This pattern is characterized by the formation of vascularized repair tissue interposed

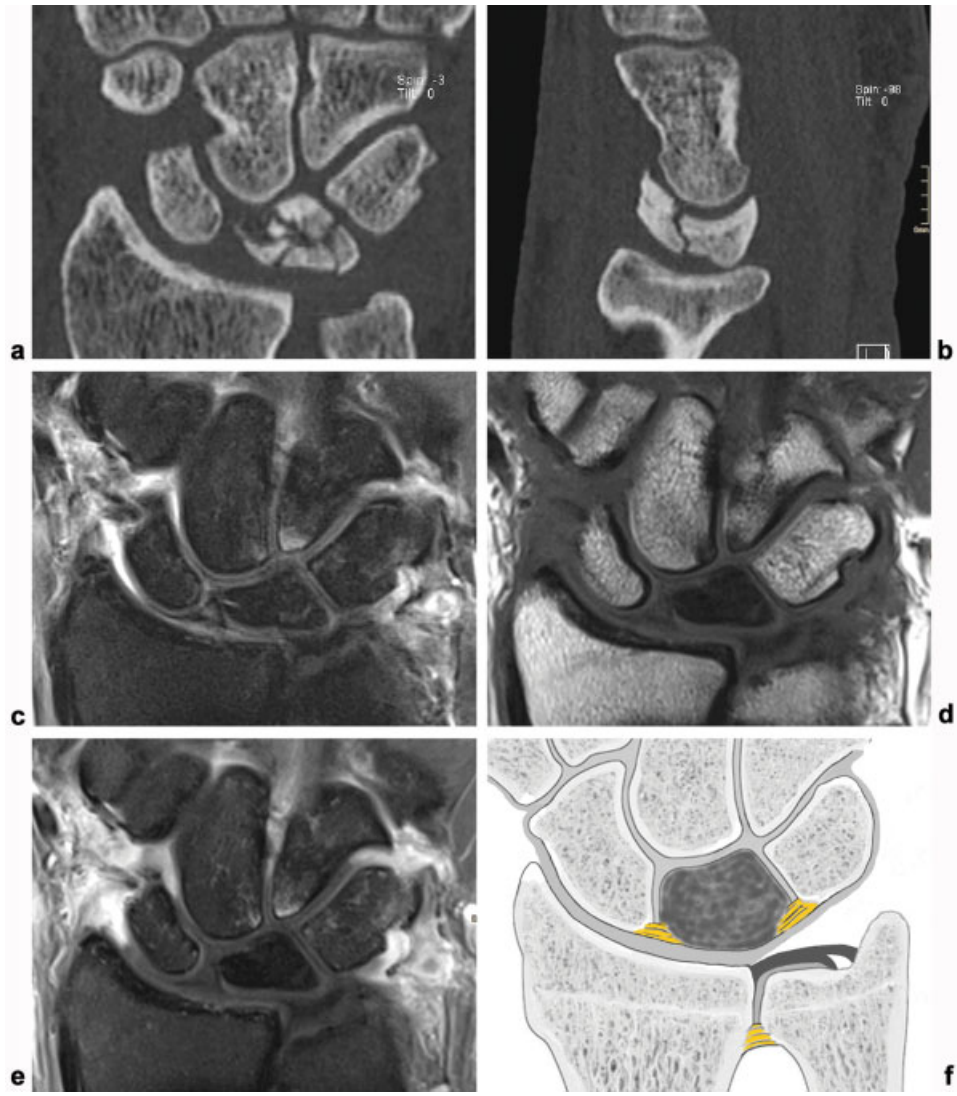

Fig. 4 Computed tomography (CT) and magnetic resonance imaging findings in perfusion pattern C of lunate necrosis. (**a**, **b**) CT imaging (coronal and sagittal multiplanar reformation) shows a fragmented pathologic fracture including coronal fracture in the sclerosed lunate. Focal loss of the articular cartilage height in the radiolunate joint. (**c**, **d**) The fractured lunate appears strongly hypointense in fat-saturated proton-density fat-saturated (FSE) (c) and plain T1 FSE images (d) as an indication of a complete loss of white fat marrow. Secondary finding: focal impingement at the tip of the hamate bone. (**e**, **f**) After gadolinium application, no hyperenhancement is present in the lunate (e) as an indication of avascularity in osteonecrosis of the entire lunate. The schematic drawing (f) illustrates the absence of residual vascularization.

between necrosis and viable bone. In plain T1-weighted sequences, necrosis and repair zones both present low signal intensity and therefore cannot be distinguished. Through intravenous administration of gadolinium, the discrimination of avascular necrosis, adjacent hypervascular repair zone, and regular bone marrow is possible.

- MRI pattern C (►**Fig. 4**): The lunate bone shows no signal after use of contrast media due to lack of repair processes. Characteristic of this pattern are extensive areas of necrosis with empty osteocyte vacuoles in histologic examination.

Differential diagnoses: In our patient population,[32] only 25.1% of signal alterations in the lunate bone could be attributed to osteonecrosis. ►**Table 1** summarizes potential differential diagnoses and their prominent characteristics.[32–36]

Osteonecrosis of the Proximal Fragment in Scaphoid Nonunion

Causes of scaphoid nonunion with potential osteonecrosis include overlooked fractures, insufficient immobilization, and severe displacement of bone fragments. The development of osteonecrosis in the proximal fragment is favored by the retrograde interosseous course of nutrient vessels originating from the radial artery.[3]

Progression of stages is typical in the development of scaphoid nonunion[17,37–39]:

- Stage I: The earliest, reversible stage comprises band-shaped resorption zones at the edges of fragments.
- Stage II: Emergence of resorption cysts indicates the transition to irreversible nonunion.
- Stage III: If fragment instability is present, osteosclerosis will start to manifest near the fracture either with

Table 1 Differential diagnoses of the signal compromised lunate bone

Entity	Distinctive features
Ulnocarpal impaction syndrome	Affects the proximal part of the lunate's ulnar side Often associated with ulna plus variants and TFCC and/or cartilage lesions
Ganglion cyst	Usually located near the insertions of the SL or LT ligament Cystic lesion with a sclerotic cortex interrupted by a transcortical connection to the ligament's origin
Trauma-associated contusion	Bone marrow edema without any characteristic location Bone bruise frequently affects more than one carpal bone
Lunate fracture	Mostly coronal fractures (rarely sagittal fractures) Extensive bone marrow edema
Avulsion injury	Displaced fragment located either next to the anterior/posterior horn or at the insertion of the SL or LT ligament Regional bone marrow edema
Midcarpal arthritis	Cartilage damage in the midcarpal compartment MRI signal alterations in the lunate and capitate head

Abbreviations: LT, lunotriquetral; MRI, magnetic resonance imaging; SL, scapholunate; TFCC, triangular fibrocartilage complex.

("hypertrophic nonunion") or without ("atrophic nonunion") formation of osteophytes.

- Stage IV: Thereafter, osteoarthritis starts to develop, leading to the formation of a so-called scaphoid nonunion advanced collapse (SNAC) wrist. Degeneration starts between the ulnar styloid process and the distal fragment of the scaphoid (IVa) and then spreads into the midcarpal joint between the proximal scaphoid fragment and capitate head (IVb). Finally, arthrosis also affects the capitolunate compartment (IVc).

Conventional radiography: Important projections include the dorsal-palmar and lateral view as well as Stecher's projection (dorsopalmar view of the closed fist during ulnar abduction).[17] Advanced stages of nonunion can be identified by the flexed position of the scaphoid and loss of carpal height. Osteonecrosis of the proximal scaphoid fragment can only be assumed in radiographic views based on extensive osteosclerosis.

CT: Oblique-sagittal and oblique-coronal MPR parallel to the longitudinal axis of the scaphoid[16,17] allow for early and exact depiction of bone resorption areas, osteosclerosis adjacent to the nonunion, and assessment of arthrosis in the radioscaphoid joint[39] (►**Fig. 5a**). Furthermore, these planes facilitate the quantification of fragment dislocation, which is particularly important for diagnosis of the "humpback" deformity (simultaneous extension of the proximal and flexion of the distal scaphoid fragment).

MRI: Like its role in the detection and classification of osteonecrosis of the lunate bone, ceMRI (►**Fig. 5b–d**) is used for visualization of bone marrow viability in the proximal scaphoid fragment. Accordingly, three patterns of osteonecrosis can be distinguished in the proximal fragment after scaphoid nonunion.[20,28,29,40] Excessive perfusion and bone marrow edema in viable osseous tissue result in homogeneous hyperenhancement (MRI pattern A). Partial necrosis of the proximal fragment leads to inhomogeneous gadolinium enhancement with extensive hyperemia in the repair zone (MRI pattern B). No enhancement is found in complete necrosis irrespective of bone marrow edema being present (MRI pattern C).

Differential diagnoses: The entities of ►**Table 2** must be differentiated from a scaphoid nonunion (without osteonecrosis of the proximal fragment).

Primary Osteonecrosis of the Scaphoid (Preiser's Disease)

Idiopathic osteonecrosis of the scaphoid bone is a rare condition, presumably induced by circulatory disturbances of the nutrient arteries.[3,41,42] As with the lunate bone, these vessels traverse in a retrograde direction from the distal to the proximal pole of the scaphoid. Preiser's disease is frequently associated with scaphoid hypoplasia, systemic diseases, and long-time application of corticosteroids. If osteonecrosis of the scaphoid is suspected, it is mandatory for diagnosis to rule out a previous scaphoid fracture in CT.

Diagnostic imaging: Corresponding to MRI findings in Kienböck's disease, we found the same three-layered composition of necrosis, repair zone, and viable bone tissue in our patient population with Preiser's disease.[43] Osteonecrosis is located primarily at the proximal pole with adjoining hypervascular repair tissue, whereas the distal segment of the scaphoid is composed of viable osseous tissue.

Early stages of idiopathic osteonecrosis are characterized by osteosclerosis and signal alterations in MRI[41,43] while the scaphoid's shape remains intact. In later stages, however, the proximal pole of the scaphoid displays a progressive conical deformation ("nipple sign") and in some cases insufficiency fractures.[41] The final stage of Preiser's disease represents the complete necrosis of the scaphoid bone.

Osteonecrosis of the Capitate Bone

The rare condition of osteonecrosis of the capitate bone typically manifests at the capitate head.[44,45] Like the lunate and scaphoid bone, the capitate receives its blood supply from nutrient vessels that have retrograde intraosseous courses after entering at the distal pole. Therefore, like

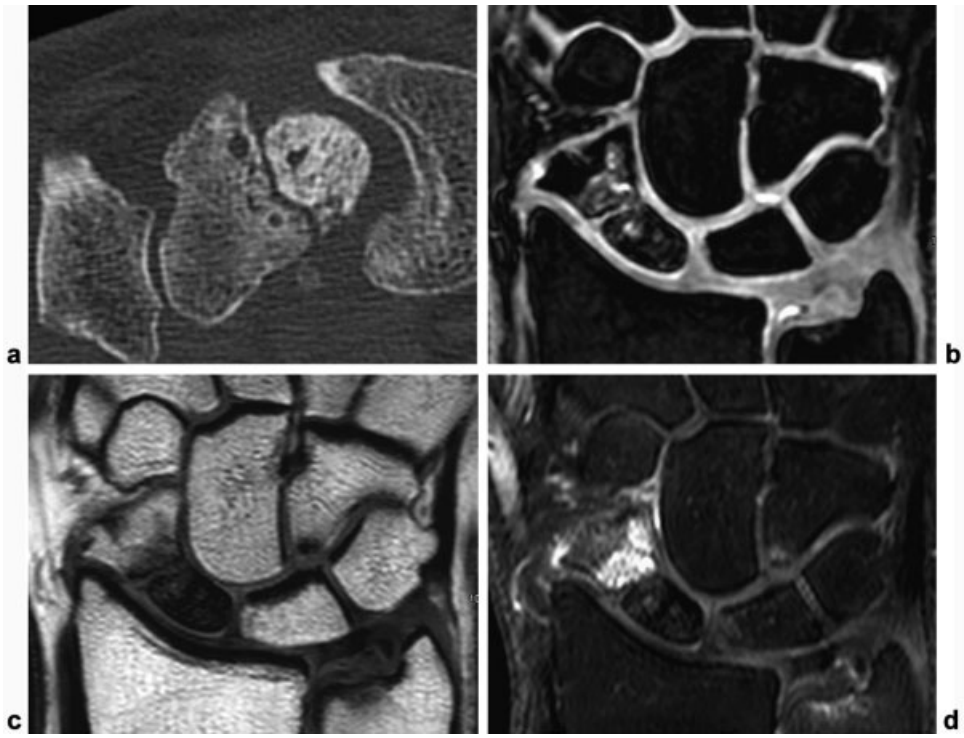

Fig. 5 Computed tomography (CT) and magnetic resonance imaging (MRI) findings in scaphoid nonunion with osteonecrosis of the proximal fragment. (**a**) Oblique-sagittal CT multiplanar reformation along the longitudinal axis of the scaphoid with evidence of proximal nonunion. Proximal fragment is osteosclerotic, both fragments contain cystic inclusions, and a dorsal osteophyte is visible on the distal fragment. (**b–d**) Coronal MRI scans: proton-density fast spin-echo (FSE) fat saturated (b), plain T1 FSE (c), and contrast-enhanced T1 FSE fat saturated (d). In the proximal scaphoid fragment, criteria of complete avitality with missing fat marrow and hyperenhancement. Adjacent hypervascular zone in distal scaphoid fragment.

the proximal segments of other carpalia, the capitate head is at particular risk of ischemia and subsequent necrosis.

Diagnostic imaging: Although uncommon, osteonecrosis of the capitate head may occur as a secondary condition in complex carpal injuries along the "greater arc," such as the rare scaphocapitate fracture syndrome (Fenton's syndrome).[46] In this injury, rotation of the capitate head by 180 degrees and consecutive interposition of articular cartilage prevents the fracture from healing while also causing circulation problems. Osteonecrosis of the capitate head is reliably visualized in ceMRI (►**Fig. 6a–d**). Progressive deformation of the capitate head is the result of insufficiency fractures in the repair zone.[45]

Osteonecrosis of the Humeral Head

Regarding the proximal upper extremity, humeral head necrosis is also subject to the pathoanatomical processes and the imaging criteria of osteonecrosis as presented in carpal bones. The humeral head presents another vascular terminal zone, supplied by intraosseous arteries of the anterolateral branch of the anterior circumflex artery that is entering the humeral head at the greater tuberosity near the intertubercular groove.[47] Occlusion of the vessel leads to ischemia of large parts of the humeral head.[48] Most frequent causes of occlusion are dislocated humeral head fractures, shoulder luxation, insertion of anchors, alcohol abuse, sickle-

Table 2 Differential diagnoses of the scaphoid nonunion

Entity	Distinctive features
Bipartite scaphoid	Separated ossification centers Ossicles of approximately equal size and density Round-shape "jointed" surfaces
Preiser's disease	Primary osteonecrosis of the (whole) scaphoid bone No trauma in patient history Pointed shape of the proximal pole ("nipple sign") Pathologic fractures mostly affect the edges of the scaphoid
Intraosseous ganglion cyst	Potentially misleading in projectional radiography Cyst with sclerosing margins and origin from the scapholunate ligament
Osteoid osteoma	Clinical symptoms similar to scaphoid nonunion Central nidus, perifocal edema, and osteosclerosis

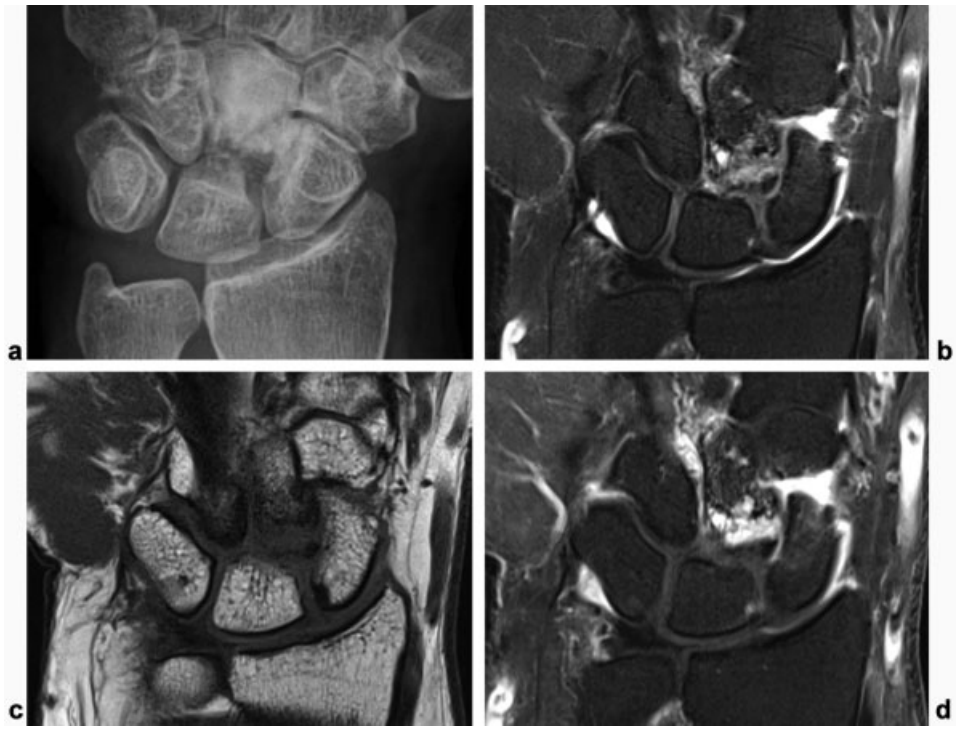

Fig. 6 Radiography and magnetic resonance imaging (MRI) in necrosis of the capitate head. (**a**) Dorsopalmar view of the wrist shows an osteolysis at the capitate head while the capitate body is condensed. (**b–d**) Coronal MRI scans: proton-density fast spin-echo (FSE) fat saturated (b), plain T1 FSE (c), and contrast-enhanced T1 FSE fat saturated (d). The capitate depicts criteria of osteonecrosis with proximal necrosis zone (hypointense in T1- and T2-weighted images and without hyperenhancement), central repair zone (edematous and hypervascular), and distal vitality zone (normal in signal height and enhancement).

cell anemia, macroglobulinemia Waldenström, antiphospholipid syndrome, corticosteroid therapy, and systemic chemotherapy.

Diagnostic imaging: The occult early stage is only visible with MRI, whereby the extent of the signal disorder correlates directly with the extent of the later osteonecrosis.[49] Osteosclerosis, subchondral fractures with loss of shape of the humeral head (►**Fig. 7a**), and finally omarthrosis follow. MRI appearance is comparable with that of femoral head osteonecrosis including the double-line sign.[48] In addition, the MRI shows the already presented zonal constitution consisting of a subchondral necrosis zone, an adjacent repair zone, and an intact head periphery (►**Fig. 7b–d**).

Bone Infarct

A bone infarct is also based on tissue necrosis with dead osteocytes. Exhibiting the same pathoanatomy, the bone infarct is distinguished from osteonecrosis only by its localization in the diaphysis or metaphysis of a long bone.[50] Clinically, bone infarctions often cause no or only minor discomfort. Biomechanically, they do not cause instability or fracturing in long bones with a strong cortical bone.

Diagnostic imaging: If the necrosis predominantly affects the fat marrow (►**Fig. 7**), a "yellow infarct" is present, characterized by a sharply defined lesion and a fat-containing center (hyperintense in T1 weighting).[50,51] If necrosis affects the normal or tumor-infiltrated hematopoietic marrow, the result is a "red infarct" with rather blurred borders and a necrotic center (hypointense in T1 weighting).

In bone infarction, a peripheral repair zone also surrounds the central necrosis area, forming three macroscopically distinguishable layers (necrosis, repair, and normal bone).[51] The repair zone is hyperintense in T2-weighted sequences and characterized by the double-line sign without fat saturation. Active repair stages are recognizable by gadolinium enhancement. With increasing infarct age, sclerosis of the repair zone occurs that is also visible in radiographs. Peripheral repair can reduce the extent of the bone infarct or make it disappear completely. The most important and sometimes difficult differential diagnosis of a bone infarct is the enchondroma.

Differential Diagnosis: Osteochondrosis

In children and adolescents, the heterogeneous disease group of osteochondrosis must be distinguished from osteonecrosis that is characterized by the death of cellular elements irrespective of age. Osteochondrosis develops at the epiphyses, apophyses, and epiphyseal plates of the growing skeleton due to developmental disorders of the bone and cartilage.[52] The cause is assumed to be a disorder of enchondral ossification due to impaired blood circulation, chronic overuse, or trauma, whereby direct osteochondral injury should be excluded. Genetic factors, skeletal dysplasia, and joint dysfunction are also discussed. Early findings are best depicted by MRI. Later, radiographic findings comprise

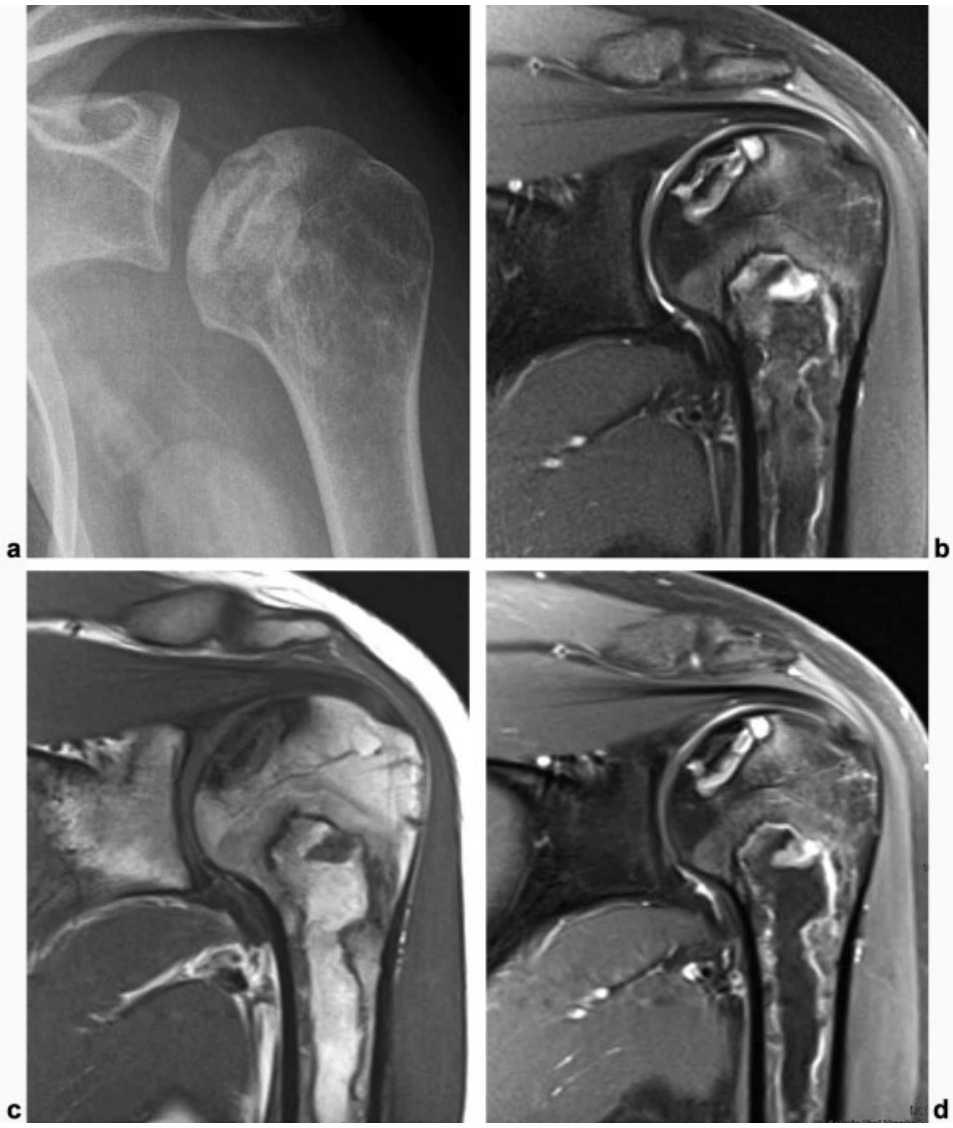

Fig. 7 Radiography and magnetic resonance imaging (MRI) in osteonecrosis of the humeral head and bone infarct in the humeral shaft. A 62-year-old female patient after chemotherapy for breast cancer with increasing pain symptoms in both shoulders. The findings of the left shoulder joint are shown, but identical image findings are also present on the right side. (**a**) True anteroposterior view of the shoulder shows an impacted fracture of the humeral head circumference in the middle segment. Fracture lines, a step in the articular surface, and subchondral osteosclerosis are present. The humeral head is decentered caudally in the glenoid cavity. The proximal section of the humerus shaft is inconspicuous. (**b**–**d**) Para-coronal MRI scans: proton-density fast spin-echo (FSE) fat saturated (b), plain T1 FSE (c), and contrast-enhanced T1 FSE fat saturated (d). In addition to the semilunar infarct zone in the middle segment of the humeral head, a tubular infarct area in the proximal humeral shaft is demarcated. The infarct center is hyperintense in plain T1 FSE indicating a so-called white infarct. In both humeral head necrosis and medullary bone infarction, peripheral hyperemia is depicted, representing marginal repair zones around the ischemic areas.

osteosclerosis, bone fragmentation, and collapse.[53] Osteochondroses are often self-limiting and resolve with remodeling or residual deformity under conservative treatment.[52] ►**Table 3** summarizes the most important osteochondroses at the upper extremity.

Discussion

The focus of this review is on osteonecrosis of the wrist, but analogies in pathoanatomy and MR imaging (three-zone model) are also shown for humeral head necrosis. Furthermore, osteochondrosis is distinguished from osteonecrosis as an independent entity.

Early and intermediate stages of osteonecrosis are not only characterized by the presence of avital "dead bone" but oftentimes display hypervascular repair zones adjacent to necrotic areas.[19,28] In these zones, hyperemia of bone marrow stimulates osteoclast (and to a lesser degree osteoblast) activity, resulting in structural remodeling of osseous tissue. The combined effects of hyperperfusion and increased bone resorption resemble the lytic stage of Paget's disease, osteopenia in transient osteoporosis or algodystrophy, as well as collateral effects of early arthritis.

Based on the retrograde intraosseous courses of nutrient arteries,[1–3] carpal bones are well suited for visualization of

Table 3 Osteochondrosis of the upper extremity

Osteochondrosis	Site	Distinctive feature
Panner's disease	Capitellum of humerus	Age 5–10 y; mostly boys Osteochondral lesions later in adolescents "Little League elbow"
Caffey's disease	Entire carpus (and other skeletal sites)	Onset at age 1 y Hypervitaminosis A and cortical hyperostosis are causative Carpal ankyloses
Mauclaire's disease	Metacarpal heads	Age 13–18 y Metacarpal head flattened Osteochondral fragments
Thiemann's disease	Phalangeal bases	Age 11–18 y; autosomal dominant Preferably proximal phalanges II, III Epiphyses sclerotic and fragmented

the mentioned three-zone model in osteonecrosis.[19,20,43] From a pathoanatomical perspective, the repair zone is characterized by the existence of hyperemia, regional osteopenia, and insufficiency fractures.

Biomechanical factors may also contribute to the development of carpal osteonecrosis because the axial load on the lunate, for instance, depends on the length ratio of the radius and ulna. In Kienböck's disease, ulna minus variants are frequently observed with consecutively increased load and onset of necrosis at the proximal-radial side of the lunate.[7–9,30,31] In contrast to osteonecrosis, the ulnocarpal impaction syndrome has its predilection site at the proximal-ulnar side of the lunate, mostly associated with ulna plus variants.[34–36]

The vascularized repair zone can be precisely differentiated from contiguous necrotic tissue by means of ceMRI. Quantification of bone marrow relaxivity before and after administration of gadolinium-based contrast media hints at the state of bone metabolism in different areas.[18,20,25,43] For visualization of osteosclerosis and other subtle radiography findings (resorption zones, insufficiency fractures, initial osteoarthritis), high-resolution computed tomography (HRCT) is considered the reference standard. Therefore, comprehensive imaging analysis in carpal osteonecrosis should always consist of synoptical use of radiography, HRCT, and ceMRI.[54,55]

Conflict of Interest
None declared.

References

1 Gelberman RH, Bauman TD, Menon J, Akeson WH. The vascularity of the lunate bone and Kienböck's disease. J Hand Surg Am 1980;5(03):272–278
2 Lluch A, Garcia-Elias M. Etiology of Kienböck disease. Tech Hand Up Extrem Surg 2011;15(01):33–37
3 Gelberman RH, Menon J. The vascularity of the scaphoid bone. J Hand Surg Am 1980;5(05):508–513
4 Ståhl F. On lunatomalacia (Kienboeck's disease): a clinical und roentgenological study, especially on its pathogenesis and the late results of immobilization treatment. Acta Chir Scand 1947;126(01):1–133
5 White RE Jr, Omer GE Jr. Transient vascular compromise of the lunate after fracture-dislocation or dislocation of the carpus. J Hand Surg Am 1984;9(02):181–184
6 Schiltenwolf M, Martini AK, Mau HC, Eversheim S, Brocai DRC, Jensen CH. Further investigations of the intraosseous pressure characteristics in necrotic lunates (Kienböck's disease). J Hand Surg Am 1996;21(05):754–758
7 Hultén O. Über die Entstehung und Behandlung der Lunatumnekrose. Acta Chir Scand 1935;76:121–135
8 Gelberman RH, Salamon PB, Jurist JM, Posch JL. Ulnar variance in Kienböck's disease. J Bone Joint Surg Am 1975;57(05):674–676
9 van Leeuwen WF, Tarabochia MA, Schuurman AH, Chen N, Ring D. Risk factors of lunate collapse in Kienböck disease. J Hand Surg Am 2017;42(11):883–888.e1
10 Desser TS, McCarthy S, Trumble T. Scaphoid fractures and Kienbock's disease of the lunate: MR imaging with histopathologic correlation. Magn Reson Imaging 1990;8(04):357–361
11 Trumble TE, Irving J. Histologic and magnetic resonance imaging correlations in Kienböck's disease. J Hand Surg Am 1990;15(06):879–884
12 Aspenberg P, Wang JS, Jonsson K, Hagert CG. Experimental osteonecrosis of the lunate. Revascularization may cause collapse. J Hand Surg [Br] 1994;19(05):565–569
13 Hashizume H, Asahara H, Nishida K, Inoue H, Konishiike T. Histopathology of Kienböck's disease. Correlation with magnetic resonance and other imaging techniques. J Hand Surg [Br] 1996;21(01):89–93
14 Ogawa T, Nishiura Y, Hara Y, Okamoto Y, Ochiai N. Correlation of histopathology with magnetic resonance imaging in Kienböck disease. J Hand Surg Am 2012;37(01):83–89
15 Kalb K, Pillukat T, Schmitt R, Prommersberger KJ. Kienböck's disease in paediatric and juvenile patients [in German]. Handchir Mikrochir Plast Chir 2010;42(03):187–197
16 Hidaka Y, Nakamura R. Progressive patterns of degenerative arthritis in scaphoid nonunion demonstrated by three-dimensional computed tomography. J Hand Surg [Br] 1998;23(06):765–770
17 Coblenz G, Christopoulos G, Fröhner S, Kalb KH, Schmitt R. Scaphoid fracture and nonunion: current status of radiological diagnostics [in German]. Radiologe 2006;46(08):664, 666–676
18 Schmitt R, Heinze A, Fellner F, Obletter N, Strühn R, Bautz W. Imaging and staging of avascular osteonecroses at the wrist and hand. Eur J Radiol 1997;25(02):92–103
19 Schmitt R, Kalb K. Imaging in Kienböck's disease [in German]. Handchir Mikrochir Plast Chir 2010;42(03):162–170
20 Schmitt R, Christopoulos G, Wagner M, et al. Avascular necrosis (AVN) of the proximal fragment in scaphoid nonunion: is intravenous contrast agent necessary in MRI? Eur J Radiol 2011;77(02):222–227

21 Decoulx P, Marchand M, Minet P, Razemon JP. La maladie de Kienbock chez le mineur; étude clinique et pathogénique avec analyse de 1330 radios de poignet. Lille Chir 1957;12(02): 65–81

22 Nattrass GR, King GJ, McMurtry RY, et al. An alternative method for determination of the carpal height ratio. J Bone Joint Surg Am 1994;76:88–94

23 Youm Y, McMurthy RY, Flatt AE, Gillespie TE. Kinematics of the wrist. I. An experimental study of radial-ulnar deviation and flexion-extension. J Bone Joint Surg Am 1978;60(04):423–431

24 Friedman L, Yong-Hing K, Johnston GH. The use of coronal computed tomography in the evaluation of Kienbock's disease. Clin Radiol 1991;44(01):56–59

25 Vande Berg BC, Malghem J, Lecouvet FE, Maldague B. MRI of the normal bone marrow. Skeletal Radiol 1998;27(09):471–483

26 Sowa DT, Holder LE, Patt PG, Weiland AJ. Application of magnetic resonance imaging to ischemic necrosis of the lunate. J Hand Surg Am 1989;14(06):1008–1016

27 Reinus WR, Conway WF, Totty WG, et al. Carpal avascular necrosis: MR imaging. Radiology 1986;160(03):689–693

28 Cerezal L, Abascal F, Canga A, García-Valtuille R, Bustamante M, del Piñal F. Usefulness of gadolinium-enhanced MR imaging in the evaluation of the vascularity of scaphoid nonunions. AJR Am J Roentgenol 2000;174(01):141–149

29 Donati OF, Zanetti M, Nagy L, Bode B, Schweizer A, Pfirrmann CW. Is dynamic gadolinium enhancement needed in MR imaging for the preoperative assessment of scaphoidal viability in patients with scaphoid nonunion? Radiology 2011;260(03):808–816

30 Lichtman DM, Ross G. Revascularization of the lunate in Kienböck's disease. In: Gelberman RH, ed. The Wrist. New York, NY: Raven Press; 1994:363–372

31 Goldfarb CA, Hsu J, Gelberman RH, Boyer MI. The Lichtman classification for Kienböck's disease: an assessment of reliability. J Hand Surg Am 2003;28(01):74–80

32 Schmitt R, Christopoulos G, Kalb K, et al. Differential diagnosis of the signal-compromised lunate in MRI [in German]. RoFo Fortschr Geb Rontgenstr Nuklearmed 2005;177(03):358–366

33 Arnaiz J, Piedra T, Cerezal L, et al. Imaging of Kienböck disease. AJR Am J Roentgenol 2014;203(01):131–139

34 Cerezal L, del Piñal F, Abascal F, García-Valtuille R, Pereda T, Canga A. Imaging findings in ulnar-sided wrist impaction syndromes. Radiographics 2002;22(01):105–121

35 Imaeda T, Nakamura R, Shionoya K, Makino N. Ulnar impaction syndrome: MR imaging findings. Radiology 1996;201(02): 495–500

36 Steinborn M, Schürmann M, Staebler A, et al. MR imaging of ulnocarpal impaction after fracture of the distal radius. AJR Am J Roentgenol 2003;181(01):195–198

37 Trojan E, Jahna H. Conservative treatment of old scaphoid fractures of the hand [in German]. Arch Orthop Unfallchir 1955;47 (01):99–104

38 Vender MI, Watson HK, Wiener BD, Black DM. Degenerative change in symptomatic scaphoid nonunion. J Hand Surg Am 1987;12(04):514–519

39 Crema MD, Zentner J, Guermazi A, Jomaah N, Marra MD, Roemer FW. Scapholunate advanced collapse and scaphoid nonunion advanced collapse: MDCT arthrography features. AJR Am J Roentgenol 2012;199(02):W202-7

40 Vogl TJ, Beutel F, Wilhelm K, et al. The MRT of scaphoid pseudarthrosis with Gd-DTPA. Its staging and clinical correlation [in German]. RoFo Fortschr Geb Rontgenstr Nuklearmed 1994;161 (05):438–445

41 Lauder AJ, Trumble TE. Idiopathic avascular necrosis of the scaphoid: Preiser's disease. Hand Clin 2006;22(04):475–484; abstract vi

42 Kalainov DM, Cohen MS, Hendrix RW, Sweet S, Culp RW, Osterman AL. Preiser's disease: identification of two patterns. J Hand Surg Am 2003;28(05):767–778

43 Schmitt R, Fröhner S, van Schoonhoven J, Lanz U, Gölles A. Idiopathic osteonecrosis of the scaphoid (Preiser's disease)—MRI gives new insights into etiology and pathology. Eur J Radiol 2011;77(02):228–234

44 Prommersberger KJ, van Schoonhoven J, Lanz U. Aseptic necrosis of the capitate: a rare cause for wrist pain. Case report and review of the literature [in German]. Handchir Mikrochir Plast Chir 2000; 32(02):123–128

45 Peters SJ, Degreef I, De Smet L. Avascular necrosis of the capitate: report of six cases and review of the literature. J Hand Surg Eur Vol 2015;40(05):520–525

46 Fenton RL. The naviculo-capitate fracture syndrome. J Bone Joint Surg Am 1956;38-A(03):681–684

47 Gerber C, Schneeberger AG, Vinh TS. The arterial vascularization of the humeral head. An anatomical study. J Bone Joint Surg Am 1990;72(10):1486–1494

48 Lee JA, Farooki S, Ashman CJ, Yu JS. MR patterns of involvement of humeral head osteonecrosis. J Comput Assist Tomogr 2002;26 (05):839–842

49 Sakai T, Sugano N, Nishii T, Hananouchi T, Yoshikawa H. Extent of osteonecrosis on MRI predicts humeral head collapse. Clin Orthop Relat Res 2008;466(05):1074–1080

50 Vande Berg BC, Malghem J, Lecouvet FE, Noel H, Maldague B. MR imaging of bone infarction and epiphyseal osteonecrosis. J Belge Radiol 1997;80(05):243–250

51 Munk PL, Helms CA, Holt RG. Immature bone infarcts: findings on plain radiographs and MR scans. AJR Am J Roentgenol 1989;152 (03):547–549

52 Doyle SM, Monahan A. Osteochondroses: a clinical review for the pediatrician. Curr Opin Pediatr 2010;22(01):41–46

53 Danger F, Wasyliw C, Varich L. Osteochondroses. Semin Musculoskelet Radiol 2018;22(01):118–124

54 Lichtman DM, Pientka WF II, Bain GI. Kienböck disease: a new algorithm for the 21st century. J Wrist Surg 2017;6(01): 2–10

55 Stahl S, Hentschel P, Ketelsen D, et al. Results of a prospective clinical study on the diagnostic performance of standard magnetic resonance imaging in comparison to a combination of 3T MRI and additional CT imaging in Kienböck's disease. Eur J Radiol 2017;90(05):212–219